MULTI-FREQUENCY RADIOMETRY FOR MULTI-YEAR MONITORING OF RELATIVE WATER CONTENT IN A TEMPERATE FOREST

Florian M. Hellwig[1,2], Thomas Jagdhuber[2,3], Anke Fluhrer[2,3], Clémence Dubois[1], David Chaparro[2], Konstantin Schellenberg[1,4], María Piles[5], Christiane Schmullius[1], Dara Entekhabi[6]

[1]Friedrich Schiller University Jena, Department for Earth Observation, Jena, Germany
[2]German Aerospace Center (DLR), Microwaves and Radar Institute (HR), Wessling, Germany
[3]University of Augsburg, Institute of Geography, Augsburg, Germany
[4]Max-Planck Institute for Biogeochemistry, Department of Biogeochemical Processes, Jena, Germany
[5]University of Valencia, Image Processing Laboratory, Valencia, Spain
[6]Massachusetts Institute of Technology (MIT), Department of Civil and Environmental Engineering, Cambridge, USA

ABSTRACT

This study presents a comparison between satellite-based vegetation optical depth (VOD) from multi-frequency radiometry (X-, C- and L-band), VOD-derived relative water content (RWC) and auxiliary data (e.g., evapotranspiration and soil moisture), which are investigated for their sensitivity to water status of tree canopies under dry and wet conditions for a temperate forest in Thuringia, Central Germany. For this, we estimated RWC directly from VOD normalization assuming no major changes in vegetation biomass or plant structure during the study period (2015-2019).

Our results show that RWC seasonalities are aligned for all investigated frequencies showing its maximum in early summer when leaves and twigs of the top and low canopy are particularly wet and photosynthetically active. Investigating drought versus non-drought years, we observed that X-band RWC is the one better capturing drought status by exhibiting low values in the extreme drought year 2018 compared to the wet year 2017 while L-band RWC reflects the ecological memory from the extreme drought conditions in 2018 in year 2019 estimates.

***Index Terms*—** Radiometry, multi-frequency, forest, relative water content, vegetation optical depth, AMSR2, SMAP, Hainich National Park

1. INTRODUCTION

The years 2018 to 2020 in Germany were characterized by high temperatures and multi-year droughts, which triggered a large-scale temperate forest decline [1,2]. During water stress conditions, leaf stomata close to prevent water loss through transpiration. As the intensity and duration of drought increases, water stress causes hydraulic failure and a reduction in defense mechanisms, both of which amplify tree mortality [3,4].

One useful indicator for monitoring water stress is the relative water content (RWC), i.e. the normalized vegetation water content [3]. RWC can be estimated directly from the vegetation optical depth (VOD) parameter without first calculating the gravimetric water content assuming no major changes in vegetation biomass or plant structure [5].

In this research study, we compare satellite-based VOD and VOD-derived RWC from multi-frequency radiometry (X-, C- and L-band) with auxiliary data for a temperate forest in dry and wet conditions to investigate their connection to the water status of trees. The study site is located in a forest of the Free State of Thuringia in Germany and covers parts of the Hainich National Park (NP).

2. STUDY AREA AND DATA

Multi-frequency radiometry allows considering the RWC of different compartments of a tree due to increasing penetration depth with decreasing frequency. We use the VOD products of JAXA's AMSR2 X- (10.7 GHz) and C-band (6.9 GHz) [6,7] and NASA's SMAP L-band radiometer sensors (1.4 GHz) [8] with almost daily (~1.7 days) acquisitions at the study area (Fig. 1).

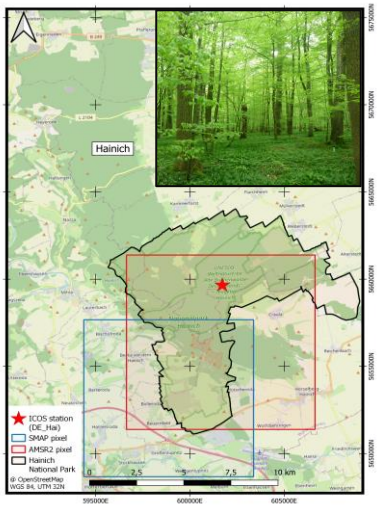

Fig. 1: Location of the study area and pixel location of the employed SMAP and AMSR2 data. The study area represents a temperate deciduous broadleaf forest in the Hainich National Park in Thuringia, Germany (10.35ºE, 51.15ºN). The vegetation image was taken by the Department of Bioclimatology (University of Göttingen) on May 5th, 2015 at the ICOS station.

DOI: https://doi.org/10.1109/IGARSS52108.2023.10281760

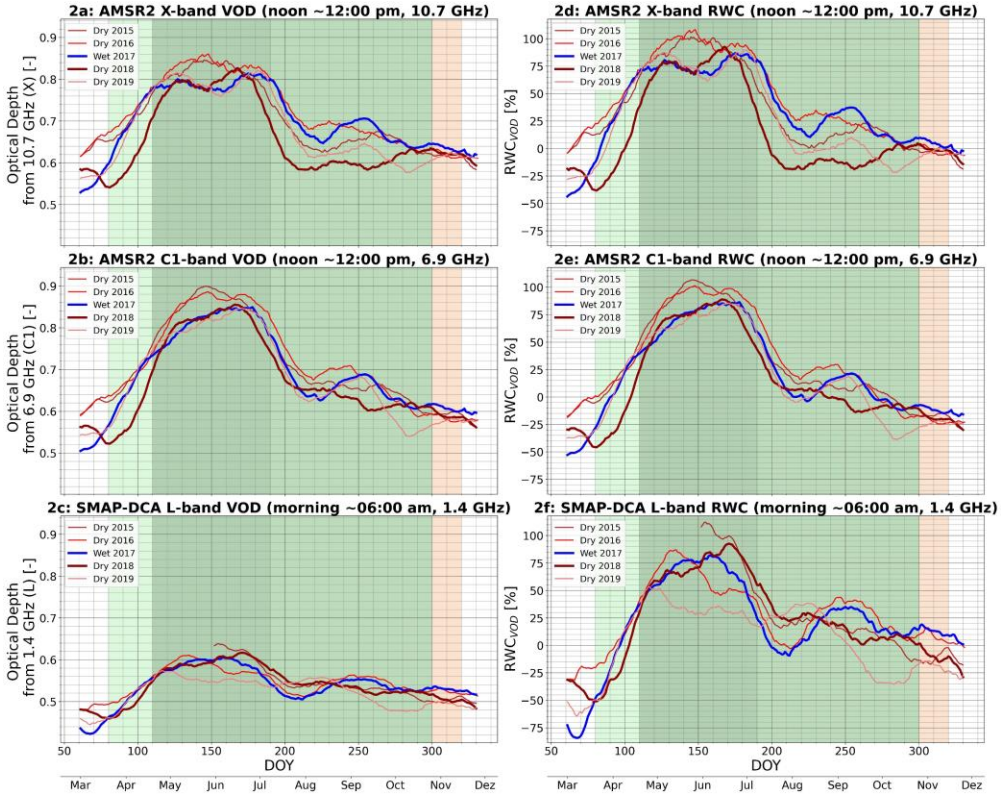

Fig. 2: Seasonal dynamics of vegetation optical depth (VOD) [Np] and relative water content (RWC) [%] derived from AMSR2 X- and C-band (10.7 and 6.9 GHz, only for noon) and auxiliary data (next page): soil moisture (SM) in a depth of 8 cm [vol. %], normalized difference moisture index (NDMI) [-], evapotranspiration (ET) [mm/d], leaf area index (LAI) [m²/m²], 95th percentile of air temperature (AT) in 2 m height [°C] and normalized difference vegetation index (NDVI) [-]. All lines are smoothed by a 31-day Savitzky-Golay filter to better recognize seasonal patterns and frost conditions were masked (DOY 1-60 and 330-365). The different years were colored based on the SPI (2017 very wet to 2018 extremely dry, blue to dark red) and the background was shaded based on four vegetation phases: spring reactivation phase (DOY 80-110, light green), high foliage phase (DOY 110-190, dark green), foliage phase (DOY 190-300, green) and defoliation phase (DOY 300-320, orange).

The coarse spatial gridding of the passive microwave data (~10 × 10 km) [6,7] limits the use to only one pixel with the highest possible coverage of forest in the Hainich NP. These pixels are covered with deciduous broadleaf forest (~51% and ~22%, primarily European beech; *Fagus sylvatica*), agricultural fields (~25 and ~39%) and pasture (~23% and ~33%) for AMSR2 and SMAP respectively [9]. Due to the acquisition geometry, the pixels shift slightly with each repetition pass. Therefore, the pixels and the land coverage percentages are not static.

For the analysis, we also use the Surface Reflectance and Leaf Area Index (LAI) products from NASA's MODIS sensor on Terra and Aqua [10, 11]. The auxiliary data (soil moisture, evapotranspiration calculated from latent heat flux and air temperature) from the nearby ICOS station (DE-Hai) [12] and precipitation data from the nearest meteorological station (DWD: Mühlhausen/Thüringen-Görmar), due to a ICOS data gap, complete the data portfolio of the study [13].

We cover the period from January 2015 to December 2019 (5 years). Based on precipitation data and its derived standard precipitation index (SPI), the period was divided into four dry (2015, 2016, 2018, 2019 for $SPI_{max} \leq -1$) and one wet year (2017 for $SPI_{max} \geq 1$) [14]. After the temporal and spatial extraction of the VOD data, the AMSR2 VOD dataset is divided into noon (~12:00 p.m.) and midnight (~01:30 a.m.) acquisitions, where we used the noon data only, because we assume that the plant-available water was replenished overnight and we see an impact of evapotranspiration at noon. Furthermore, the auxiliary data are averaged to daily mean products and tailored to the AMSR2 pixel.

3. METHODS

RWC is determined by normalizing the VOD using the 5th and 95th percentiles (VOD_{min} and VOD_{max}, respectively) over a specific time period [15]. An important prerequisite for this is no major change in vegetation biomass or plant structure [5]. To ensure this, a period of stable vegetation conditions is determined based on vegetation images and the MODIS LAI product [11]. This period (DOY 130-250) of each year, except 2018 due to extreme drought conditions, is used as the normalization period for calculating the RWC for the whole study period. Besides, four different vegetation phases are determined: spring reactivation phase (DOY 80-110), high foliage phase (DOY 110-190), foliage phase (DOY 190-300) and defoliation phase (DOY 300-320).

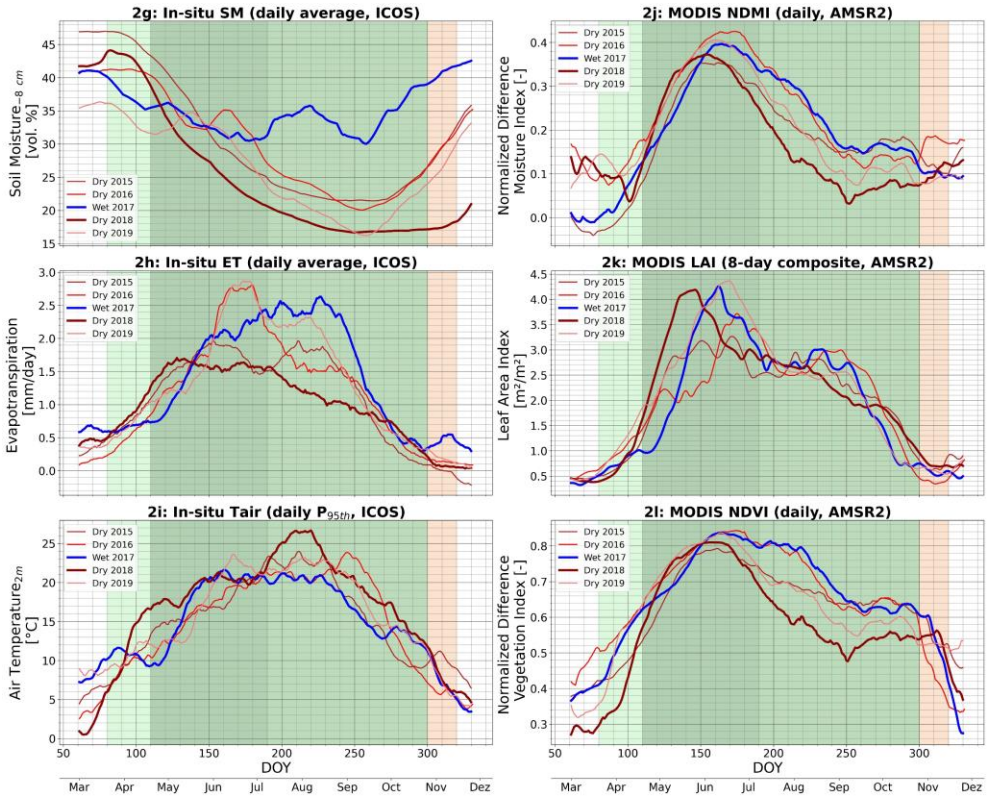

Moreover, the normalized difference vegetation index (NDVI) and the normalized difference moisture index (NDMI) were calculated based on the MODIS Surface Reflectance product (NDMI = (B2-B6)/(B2+B6), NDVI = (B2-B1)/(B2+B1)) [10].

4. RESULTS

Figure 2 shows the comparison of dry and wet years for VOD and RWC from the X-, C- and L-band together with the auxiliary data. Basically, for all bands, a high RWC (> 50%) occurs in summer for the high foliage phase (DOY 110-190). Comparing dry to wet conditions, the RWC in 2018 is clearly lower in the spring reactivation phase (DOY 80-110) and the foliage phase (DOY 190-300) for X-band and partially for C-band, while for L-band wet conditions results in a higher RWC from the end of the foliage phase only (DOY ~230-330) (Fig. 2d-f). Correspondingly, the same applies to VOD (Fig. 2a-c).

Regarding the auxiliary data, higher air temperature (AT) occurs in drought years, especially in April to May and August to September (Fig. 2i). Soil moisture (SM) generally decreases from April to September. While under wet conditions SM does not fall below ~30 vol. % even in summer, dry periods bring the topsoil down to ~17 vol. %. For the extreme drought year 2018 SM does not recover over winter but stays on lower level (~30 vol. %) (Fig. 2h). Furthermore, for extremely dry conditions, evapotranspiration (ET) is considerably reduced (<1.5 mm/day) in contrast to wet conditions (>2 mm/day), particularly between July to August (Fig. 2g). In addition, the different vegetation indices roughly follow the vegetation phases, i.e. the indices rise and fall with the development of vegetation (Fig. 2j-l).

5. DISCUSSION AND OUTLOOK

Drought conditions strongly reduce topsoil SM from late summer to winter, inducing a hydrological drought and high spring/early summer AT in drought years lead to an earlier start of the vegetation period (LAI) and results in lower ET. We find X-band RWC to correspond to drought-related variables by exhibiting low values in the extreme drought year 2018 compared to the wet year 2017 (Figure 2). This may be explained by water stress causing leaf desiccation, reducing ET and thus the photosynthetic activity [3], which is also confirmed by the LAI fall in summer (Fig. 2k).

Moreover, we assume that the short X- and C-band waves interact mostly with the leaves and twigs of the top canopy. Therefore, X- and C-band RWC is the highest in early summer when these tree components are particularly wet and active (high foliage phase). Further indication of this is provided by the indices of the optical remote sensing data, which show a high biomass and water content at the same time as well as a similar course over the year. As RWC increases already in the spring reactivation phase before canopy foliation, a correlation with plant water uptake and understory development is conceivable.

Furthermore, we assume that the longer L-band waves interact mainly with branches and trunks of the lower canopy.

This can explain the differences between L-band RWC seasonality with respect to X- and C-band ones. Additionally, the L-band may reflect ecological memory from past drought conditions in low tree compartments, as we observed the L-band RWC of 2019 (one year after extreme drought) is clearly lower in the high foliage phase (DOY 110-190).

Previous studies have recommended the use of high-frequency bands (C-, X- and Ku-band) instead of L-band to derive leaf-related variables, like the degree of isohydricity [17], the gross primary production (GPP; [17]) or the life fuel moisture content (LFMC; [18]). However, adding L-band can be helpful to interpret the behavior of VOD and RWC, especially in pixels with heterogeneous land cover [19] such as the ones in the Hainich NP. We hypothesize the difference between low and high frequency RWC for dry and wet years could point towards different water dynamics of the different tree compartments during the vegetation period.

However, it has to be noted that the assumption of no biomass variability holds only partially in the study area. Even if a particular constant biomass period is used for VOD normalization, it is difficult to fully control the influence of this factor. Instead, the retrieved RWC can be partially affected by biomass changes along time, suggesting that complementing this analysis with in situ or remotely sensed vegetation moisture information should be a next step in this research.

In summary, simultaneous multi-year and multi-frequency radiometry is crucial to monitor different tree compartments and thus water stress in (complex) forest canopies. For long-term observations, it would be desirable to obtain several frequencies at the same time of the day, e.g. as will be provided by the upcoming CIMR mission carrying Ka-, K-, X-, C- and L-band sensors [20], as well as a higher temporal and spatial resolution compared to currently operating space-borne radiometers.

6. REFERENCES

[1] Buras, A., Rammig, A., & Zang, C. S. (2020). Quantifying impacts of the 2018 drought on European ecosystems in comparison to 2003. *Biogeosciences*, *17*(6), 1655–1672. https://doi.org/10.5194/bg-17-1655-2020.

[2] Thonfeld, F., Gessner, U., Holzwarth, S., Kriese, J., da Ponte, E., Huth, J., & Kuenzer, C. (2022). A First Assessment of Canopy Cover Loss in Germany's Forests after the 2018–2020 Drought Years. *Remote Sensing*, *14*(3), 562. https://doi.org/10.3390/rs14030562.

[3] Konings, A. G., Saatchi, S. S., Frankenberg, C., Keller, M., Leshyk, V., Anderegg, W. R. L., . . . Zuidema, P. A. (2021). Detecting forest response to droughts with global observations of vegetation water content. *Global Change Biology*, *27*(23), 6005–6024. https://doi.org/10.1111/gcb.15872.

[4] McDowell, N., Pockman, W. T., Allen, C. D., Breshears, D. D., Cobb, N., Kolb, T., . . . Yepez, E. A. (2008). Mechanisms of plant survival and mortality during drought: Why do some plants survive while others succumb to drought? *The New Phytologist*, *178*(4), 719–739. https://doi.org/10.1111/j.1469-8137.2008.02436.x

[5] Jagdhuber, T., Jonard, F., Fluhrer, A., Chaparro, D., Baur, M. J., Meyer, T., & Piles, M. (2022). Toward estimation of seasonal water dynamics of winter wheat from ground-based L-band radiometry: a concept study. *Biogeosciences*, *19*(8), 2273–2294. https://doi.org/10.5194/bg-19-2273-2022.

[6] Jeu, R. de & Owe, M. (2014). AMSR2/GCOM-W1 surface soil moisture (LPRM) L3 1 day 10 km x 10 km ascending V001 [Data set]. Edited by Goddard Earth Sciences Data and Information Services Center (GES DISC) (Bill Teng), Greenbelt, MD, USA, Goddard Earth Sciences Data and Information Services Center (GES DISC). Accessed 2022-11-02 from https://doi.org/10.5067/B0GHODHJLDA8.

[7] Owe, M., Jeu, R. de & Holmes, T. (2008). Multisensor historical climatology of satellite-derived global land surface moisture. *Journal of Geophysical Research*, *113*(F1), 687.

[8] O'Neill, P. E., Chan, S., Njoku, E. G., Jackson, T., Bindlish, R. & Chaubell, J. (2020). SMAP Enhanced L3 Radiometer Global Daily 9 km EASE-Grid Soil Moisture, Version 4 [Data Set]. Boulder, Colorado USA. NASA National Snow and Ice Data Center Distributed Active Archive Center. https://doi.org/10.5067/NJ34TQ2LFE90. Date Accessed 02-24-2023.

[9] EEA & Copernicus programme (2020). Corine Land Cover (CLC) 2018 (Version 2020_20u1) [Data set]. Accessed 2022-11-16 from https://land.copernicus.eu/pan-european/corine-land-cover/clc2018.

[10] Lyapustin, A. & Wang Y. (2022). MODIS/Terra+Aqua Land Surface BRF Daily L2G Global 500m and 1km SIN Grid V061 [Data set]. NASA EOSDIS Land Processes DAAC. Accessed 2023-03-29 from https://doi.org/10.5067/MODIS/MCD19A1.061.

[11] Myneni, R., Knyazikhin, Y. & Park, T. (2015). MOD15A2H MODIS/Terra Leaf Area Index/FPAR 8-Day L4 Global 500m SIN Grid V006 [Data set]. NASA EOSDIS Land Processes DAAC. Accessed 2022-11-03 from https://doi.org/10.5067/MODIS/MOD15A2H.006.

[12] Knohl, A., Siebicke, L., Tiedemann, F., Kolle, O., & ICOS Ecosystem Thematic Centre. (2022). Warm winter 2020 ecosystem eddy covariance flux product from Hainich (Version 1.0) [Data set]. ICOS Carbon Portal. Accessed 2022-11-02 from https://doi.org/10.18160/CR66-PJ24.

[13] DWD (2021). Opendata. Mühlhausen/Thüringen-Görmar [Data set]. Accessed 2022-11-02 from https://opendata.dwd.de/climate_environment/CDC/observations_germany/climate.

[14] WMO (2012). Standardized Precipitation Index User Guide. WMO No. 1090. Geneva, Switzerland.

[15] Rao, K., Anderegg, W.R.L., Sala, A., Martínez-Vilalta, J. & Konings, A.G. (2019). Satellite-based vegetation optical depth as an indicator of drought-driven tree mortality. *Remote Sens. Environ.*, 227, 125–136.
https://www.sciencedirect.com/science/article/pii/S0034425719301208.

[16] Konings, A. G., & Gentine, P. (2017). Global variations in ecosystem-scale isohydricity. *Global Change Biology*, *23*(2), 891–905. https://doi.org/10.1111/gcb.13389.

[17] Teubner, I. E., Forkel, M., Jung, M., Liu, Y. Y., Miralles, D. G., Parinussa, R., . . . Dorigo, W. A. (2018). Assessing the relationship between microwave vegetation optical depth and gross primary production. *International Journal of Applied Earth Observation and Geoinformation*, *65*(10), 79–91. https://doi.org/10.1016/j.jag.2017.10.006.

[18] Forkel, M., Schmidt, L., Zotta, R.-M., Dorigo, W., & Yebra, M. (2023). Estimating leaf moisture content at global scale from passive microwave satellite observations of vegetation optical depth. *Hydrology and Earth System Sciences*, *27*(1), 39–68. https://doi.org/10.5194/hess-27-39-2023.

[19] Olivares-Cabello, C., Chaparro, D., Vall-llossera, M., Camps, A., & López-Martínez, C. (2022). Global Unsupervised Assessment of Multifrequency Vegetation Optical Depth Sensitivity to Vegetation Cover. *IEEE Journal of Selected Topics in Applied Earth Observations and Remote Sensing*, *16*, 538-552. https://doi.org/10.1109/JSTARS.2022.3226001.

[20] Donlon et. al (2023). CIMR Mission Requirements Document v5.0. Accessed 2023-02-11 from https://esamultimedia.esa.int/docs/EarthObservation/CIMR-MRD-v5.0-20230211_(Issued).pdf.